MRS Advances © 2018 Materials Research Society
DOI: 10.1557/adv.2018.171

Downloaded from https://www.cambridge.org/core. IP address: 24.242.98.122, on 13 Feb 2018 at 03:49:54, subject to the Cambridge Core terms of use, available at https://www.cambridge.org/core/terms. https://doi.org/10.1557/adv.2018.171

Electron Spin Resonance Investigations on Perovskite Solar Cell Materials Deposited on Glass Substrate

C. L. Saiz[1], E. Castro[2], L. M. Martinez[1], S. R. J. Hennadige[2], L. Echegoyen[2], S. R. Singamaneni[1]

[1]*Department of Physics, The University of Texas at El Paso, El Paso, Texas 79968, USA.*

[2]*Department of Chemistry, The University of Texas at El Paso, El Paso, Texas 79968, USA.*

ABSRTACT

In this article, we report low-temperature electron spin resonance (ESR) investigations carried out on solution processed three-layer inverted solar cell structures: $PC_{61}BM/CH_3NH_3PbI_3$/PEDOT:PSS/Glass, where $PC_{61}BM$ and PEDOT:PSS act as electron and hole transport layers, respectively. ESR measurements were conducted on ex-situ light (1 Sun) illuminated samples. We find two distinct ESR spectra. First ESR spectra resembles a typical powder pattern, associated with $g_x = g_y = 4.2$; $g_z = 9.2$, found to be originated from Fe^{3+} extrinsic impurity located in the glass substrate. Second ESR spectra contains a broad (peak-to-peak line width ~ 10 G) and intense ESR signal appearing at g = 2.008; and a weak, partly overlapped, but much narrower (peak-to-peak line width ~ 4 G) ESR signal at g = 2.0022. Both sets of ESR spectra degrade in intensity upon light illumination. The latter two signals were found to stem from light-induced silicon dangling bonds and oxygen vacancies, respectively. Our controlled measurements confirm that these centers were generated during UV-ozone treatment of the glass substrate –a necessary step to be performed before PEDOT:PSS is spin coated. This work forms a significant step in understanding the light-induced- as well as extrinsic defects in perovskite solar cell materials.

INTRODUCTION

Polycrystalline thin films of $CH_3NH_3PbI_3$ ($MAPbI_3$), being the dominant form of photovoltaic applications, have drawn a great deal of scientific and technological interest due to a boost in performance from 3.8% in 2005 to a record high 22.1% power conversion efficiency in 2015, exceptional electron-hole diffusion length (>1 μm), and high open circuit voltage of >1 V [1]. Most importantly, these materials are cheap to fabricate using simple low temperature solution-based methods, and employ 1000-times less light harvesting material compared to the current market leader, polycrystalline silicon, with efficiency > 25%. Despite these extraordinary properties, under normal solar operating conditions in open air, $MAPbI_3$ turns into a photo-inactive yellow phase and can no longer be used for photovoltaic applications. Due to defect formation and ion migration, $MAPbI_3$

degrades relatively rapidly and becomes highly unstable [2]. In addition, $MAPbI_3$-based materials are vulnerable to degradation by external stimuli such as prolonged light illumination [3]. Although many advances are being reported to control degradation, literature reports that solar power conversion efficiencies are inconsistent and often irreproducible, leading to ever growing and unsettled debates [4]. The above key issues remain a significant challenge, and impede the commercial applications, as widely discussed in many reviews [4, 5]. To our knowledge, work to address the processing induced effects in $MAPbI_3$ materials have not been reported, which is the motivation for this work.

To address the above issues, many theoretical and experimental efforts were made to investigate defect formation and identification in these solar cell materials [6]. Previous researchers [7] have used several techniques such as admittance spectroscopy, thermally simulated current measurements, and confocal optical microscopy to characterize the defects present in these materials. However, these techniques have no capability to atomically identify the defects, particularly those that are associated with unpaired electron spins. ESR spectroscopy can be an ideal local experimental technique to investigate the microscopic details of solar cell material performance upon external perturbations. In the recent past, ESR spectroscopy has been successfully employed to better understand the performance of polymer solar cell materials [9]. To date, there has been very limited work reported that investigate the point defects that arise during the fabrication process of perovskite solar cells using the ESR technique [10,11]. For instance, Shkrobe et al. studied [10] the charge trapping process in bulk polycrystals of photovoltaically active perovskites and related halogenoplumbate compounds using ESR spectroscopy. They demonstrated that the holes are trapped by organic cations whereas Pb^{2+} centres trap electrons. In a more recent work [11], Namatame and co-authors employed room-temperature ESR spectroscopy to observe dramatic enhancement of hole formation in a perovskite solar cell material spiro-OMeTAD by Li-TFSI doping. In addition, they observed photo generated spins upon *in-situ* light irradiation. However, the above studies did not address how the steps involved in the solar cell material deposition process affect the ESR spectral behavior.

The present work focuses on previously unreported ESR studies performed at cryogenic temperatures (10 K) conducted on $MAPbI_3$-based thin film structures deposited on glass substrates. ESR measurements were performed on pristine layers as well as light (1 Sun) illuminated layers. We detected two-sets of ESR spectra where their intensities decreased drastically upon illumination. We assign the first set of ESR spectra to the Fe^{3+} impurity present in the glass substrate. Our controlled measurements infer that the second set of paramagnetic centres found in the samples were generated during UV-ozone treatment (30 min) of the glass substrates –a necessary step performed before PEDOT:PSS spin-coating.

EXPERIMENTAL DETAILS

In-depth details on the preparation and characterization of solar cell materials for the present study were reported earlier by some of us [12,13]. J-V characteristics of $MAPbI_3$-based photovoltaic solar cells were tested [12] using a Keithley 2420 source meter under a Photo Emission Tech SS100 solar simulator. Light intensity was calibrated by a standard Si solar cell. Film thicknesses were measured using a KLA Tencor profilometer. Ex-situ light illumination was carried out from the back side of the glass substrate using the solar simulator under ambient air. The ESR data were recorded on a Bruker EMX Plus X-band ESR Spectrometer equipped with a high sensitivity probe head. A ColdEdge™ ER

Downloaded from https://www.cambridge.org/core. IP address: 24.242.98.122, on 13 Feb 2018 at 03:49:54, subject to the Cambridge Core terms of use, available at https://www.cambridge.org/core/terms. https://doi.org/10.1557/adv.2018.171

4112HV In-Cavity Cryo-Free VT system connected with an Oxford temperature controller was used for low temperature measurements. The complete system was operated by Bruker Xenon software. Sample dimensions were 3 mm x 20 mm for all measurements. In addition, all ESR experimental settings were kept constant for reproducibility and consistency. ESR settings: modulation amplitude = 2 G (peak-to-peak), modulation frequency = 100 kHz. The magnetic field was applied parallel to the surface normal of the film plane. All layers were un-encapsulated during measurement.

RESULTS AND DISCUSSION

All ESR experiments were performed at cryogenic temperature of 10 K to gain maximum sensitivity. X-band ESR measurements were conducted on as fabricated $PC_{61}BM/MAPbI_3$/PEDOT:PSS/Glass heterostructures without external light illumination (referred to as dark). Figure 1(a) shows representative ESR spectra recorded from 0-6000 G. This plot shows two sets of signals appearing at low (500-2500 G –first set) and high (3320-3380 G –second set) magnetic field regions, which will be discussed later on. We verified that these spectra didn't originate from the ESR cavity background or from the quartz tube that was used to load the samples. In addition, we find that these signals are entirely different from the signals reported in the literature [11] for thin films of $MAPbI_3$/spiro-OMeTAD after doping with Li-TFSI source, and *in-situ* irradiated polycrystalline PbI materials. $MAPbI_3$ has an absorption coefficient roughly in the range of 104-105 cm^{-1}. This will allow most incident light to be absorbed in the film with the thickness range of 300-500 nm.

We now discuss the effect of *ex-situ* illumination on the ESR spectra. ESR spectra recorded on the sample under dark condition is shown in Fig. 1(a). In Figure 1(b), we plot the ESR spectra collected for the above structures as a function of illumination time from 0.25-4.5 hrs. Contrary to our anticipation, we detected no additional ESR lines upon illumination throughout the magnetic field range in comparison with the ESR spectra recorded under dark (see, Fig. 1(a)). This observation indicates that the Pb clusters, organic, and inorganic cations [10,11] (if at all they are formed) might have decayed rapidly (if they are formed) or went undetected at our measured x-band microwave frequency as we employed ex-situ illumination**.** It also infers that this material is free from secondary phases, thus corroborating previously published data [12,13].

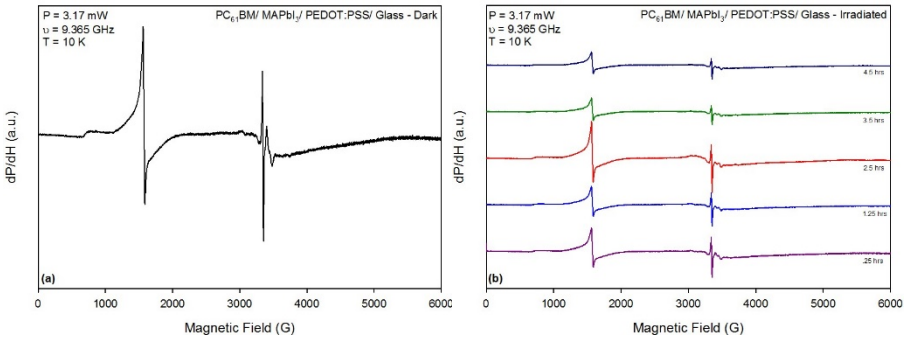

Figure 1(a). First derivative ESR spectra collected from $PC_{61}BM/MAPbI_3$/PEDOT:PSS/Glass under no light illumination (dark). **Figure 1(b)**. Comparison of first derivative ESR spectra plotted as a function of light illumination time.

Downloaded from https://www.cambridge.org/core. IP address: 24.242.98.122, on 13 Feb 2018 at 03:49:54, subject to the Cambridge Core terms of use, available at https://www.cambridge.org/core/terms. https://doi.org/10.1557/adv.2018.171

Next, we analyzed the signals appearing on the low field region as shown in Fig. 2. These spectra exhibit a typical powder pattern, characterized by $g_x = g_y = 4.2$, $g_z = 9.3$. Based on g-values reported in the literature works [18, **19**] together with our controlled measurements, we established that these signals originate from the glass substrate itself and not from the other layers. We assigned these spectra to an unexpected Fe^{3+} (high-spin, S = 5/2, I = 0) ion, which is octahedrally (six-fold) coordinated with oxygen ions present in the glass substrate. The signal appearing at g = 4.2 is associated with $|\pm 3/2>$ doublet of the S = 5/2 system with the rhombicity of 1/3. The weak signal originating at g = 9.3 is due to $|\pm 1/2>$ doublet of the S = 5/2 system. Upon illumination, the intensity of Fe^{3+} signal is reduced drastically (see, Fig. 2), although the intensity of ESR signals due to the Fe^{3+} impurity centres in irradiated glasses are not expected to change [14]. At this moment, we do not know the origin of Fe^{3+} signal intensity reduction upon illumination. No paramagnetic ESR signal was observed either from the pristine nor the irradiated layers of $MAPbI_3$, PEDOT:PSS, or $PC_{61}BM$. We note here that the signal of conduction electron spin resonance (CESR) generated by the illumination is not detected either. That may be due to low Pauli spin susceptibility of a CESR signal, and the strong spin–orbit coupling [15] of Pb and iodine that may broaden the signal beyond detection.

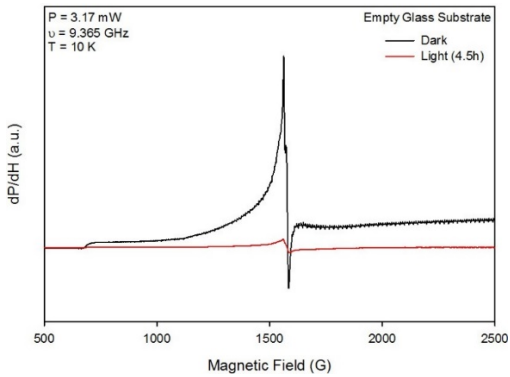

Figure 2. Enlarged first derivative ESR spectra collected from $PC_{61}BM$ /$MAPbI_3$/PEDOT:PSS/Glass, before and after light illumination for 4.5 hrs.

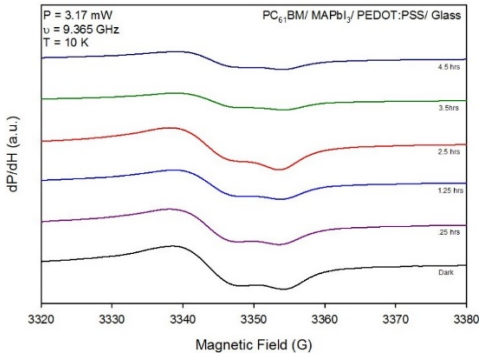

Figure 3. Enlarged high field ESR spectra collected as a function of light illumination time, including the spectra measured under dark conditions.

Downloaded from https://www.cambridge.org/core. IP address: 24.242.98.122, on 13 Feb 2018 at 03:49:54, subject to the Cambridge Core terms of use, available at https://www.cambridge.org/core/terms. https://doi.org/10.1557/adv.2018.171

The high field region data as a function of illumination time, shown in Fig. 3, shows two partially overlapped ESR signals appearing at g = 2.0081, and g = 2.0030, which exhibit a Lorentzian line shape. The peak-to-peak linewidths of these two signals are ~ 10 G and 4 G, respectively. Interestingly, the intensity of these signals diminished as a function of illumination time, though non-monotonically. No new signals were observed nor did the existing signals disappear. It is also noted that no hyperfine structure was observed that might correspond to isotopes of Pb or methylene cations that might have been formed during the irradiation [10].

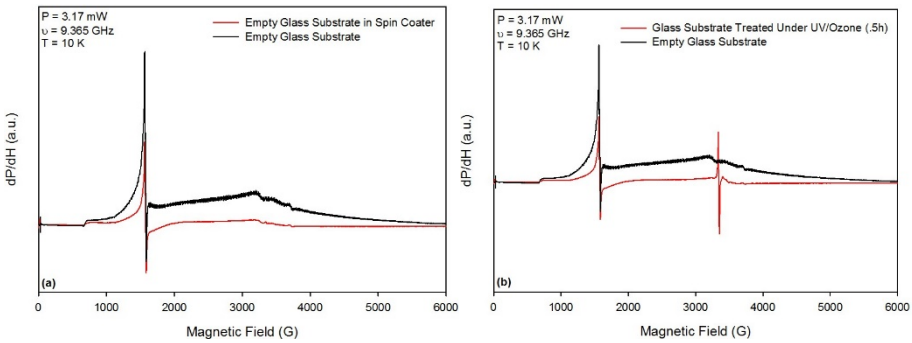

Figure 4(a). ESR spectra of pristine glass substrate and with glass substrate exposed to spin coater for standard time. **Figure 4(b)**. Comparison of ESR spectra collected from the pristine and UV-ozone treated glass substrate.

To trace the origin of these signals, we next investigated the layers in a more systematic manner. We collected ESR spectra on single layer samples, before and after illumination. To our surprise, the same set of signals were observed from all samples that were measured. These experimental findings led us to believe that these signals do not originate from any of the three layers deposited on the glass substrates. In addition, we find no signal that might have originated from the contamination of the glass during the spin coating process (Fig. 4(a)). As shown in Figure 4(b), we found precisely the same signals for the UV-ozone treated glass substrate by itself. The ESR spectra are consistent with those observed for the illuminated $PC_{61}BM/MAPbI_3/PEDOT:PSS/Glass$ (Fig. 3). It should be mentioned that UV-ozone treatment is an essential step performed before the deposition of the over layers. Upon comparing these signals with those reported in the literature [16], we identified that the signal appearing at g = 2.008 is due to silicon dangling bonds. The signal at g = 2.003 is due to oxygen vacancies. Except for the decrease in signal intensity, all other ESR spectral parameters such as linewidth and g-value remain constant.

As mentioned before, we recorded ESR spectra on single layers of $PC_{61}BM$, $MAPbI_3$, and PEDOT:PSS. We detected no ESR signals that were expected [17] from $PC_{61}BM$ (g_x = 2.0060, g_y = 2.0028, g_z = 2.0021), or PEDOT:PSS [8] (g = 2.0037) before and after illumination. We observed no photo generated carbon dangling radicals [17] with a g-value of 2.0029 which clearly establishes that the signals we observed did not originate from the over layers. Therefore, the only source that can give rise to such signals is the underlying UV-ozone treated glass substrate. It should be noted that we could not rule out the formation of spin centers with a spin lifetime less than 10 μs as we are bound to use 100 kHz modulation frequency for X-band ESR measurements. Our initial low temperature (4 K), high frequency (~ 120 GHz) ESR measurements (data not shown) performed at National High Magnetic Field Laboratory (NHMFL, FL) did not reveal any new signals upon *ex-situ* illumination, which is similar to the results obtained at X-band (9.365 GHz) frequency.

Downloaded from https://www.cambridge.org/core. IP address: 24.242.98.122, on 13 Feb 2018 at 03:49:54, subject to the Cambridge Core terms of use, available at https://www.cambridge.org/core/terms. https://doi.org/10.1557/adv.2018.171

CONCLUSION

We have reported X-band ESR investigations carried out on inverted perovskite solar cell structures: PC61BM/MAPbI3/PEDOT:PSS/Glass. ESR measurements were performed at the cryogenic temperature (10 K) on pristine and *ex-situ* illuminated samples. Two distinct ESR spectra were observed. The signal with gx = gy = 4.2; gz = 9.2, was assigned to unexpected Fe^{3+} ions located in the glass substrate. The second set of signals shows a broad and intense ESR signal at g = 2.005-2.008; and a weak, but much sharper ESR signal at g = 2.0022. The intensities of both sets of ESR signals decreased upon illumination for 4.5 hrs, whose origin is unknown at this point. We found that the latter two ESR lines stem from silicon dangling bonds and oxygen vacancies, respectively. Detailed measurements indicate that silicon dangling bonds and oxygen vacancies were generated during UV-ozone treatment of the glass substrate –a necessary step to be performed before PEDOT:PSS is spin coated**.** This work shows the importance of closely looking at the process-induced effects on solar cell substrates using spin-sensitive local experimental probes such as ESR spectroscopy.

ACKNOWLEDGEMENTS

C.L.S, L.M.M, and S.R.S acknowledge support from a UTEP start-up grant. L.M.M and S.R.S acknowledge the Wiemer Family for awarding Student Endowment for Excellence. S.R.S and L.E. thank the NSF-PREM program (DMR – 1205302). L.E. thanks the NSF grant CHE-1408865 and the Robert A. Welch Foundation is also gratefully acknowledged for an endowed chair to L.E. (grant AH-0033).

REFERENCES

1. G. Xing, N. Mathews, S. Sun, S. S. Lim, Y. M. Lam, M. Grätzel, S. Mhaisalkar, T. C. Sum. Sci. 342, 344–347 (2013).
2. Y. Shao, Z. Xiao, C. Bi, Y. Yuan, J. Huang. Nat. Comm. 5, 57845791 (2014).
3. W. Hao, X. Chen, and S. Li. J. Phys. Chem. C, 120, 28448−28455, (2016).
4. Y. Yang and J. You. Nature 544, 155-156 (2017).
5. Dirk C. Jordan, T. J. Silverman, J. H. Wohlgemuth, S. R. Kurtz and K. T. VanSant. Prog. Photovolt: Res. Appl. 25, 318–326 (2017).
6. W-J Yin, T. Shi, and Y. Yan. Appl. Phys. Lett., 104, 063903-063907 (2014).
7. H-S Duan, H. Zhou, Q. Chen, P. Sun, S. Luo, T-B Song, B. Bob and Y. Yang. Phys. Chem. Chem. Phys. 17, 112 (2014).
8. D. W. deQuilettes, S. M. Vorpahl, S. D. Stranks, H. Nagaoka, G. E. Eperon, M. E. Ziffer, H. J. Snaith, D. S. Ginger. Science 348, 683-686 (2015).
9. J-K Lee, S. You, S. Jeon, N-H Ryu, K. H. Park, K. Myung-Hoon, D. H. Kim, S. H. Kim, and Eric A. Schiff. J. Appl. Phys. 118, 015501-015507 (2015).
10. I. A. Shkrob, and T. W. Marin. J. Phys. Chem. Lett., 5, 1066−1071 (2014).
11. M. Namatame, M. Yabusaki, T. Watanabe, Y. Ogomi, S. Hayase, and K. Marumoto. Appl. Phys. Lett., 110, 123904-123909 (2017).
12. C. Tian, E. Castro, T. Wang, G. Betancourt-Solis, G. Rodriguez, and L. Echegoyen. ACS Appl. Mater. Interfaces, 8, 31426−31432 (2016).
13. C. Tian, K. Kochiss, E. Castro, G. Betancourt-Solis, H. Hanb and L. Echegoyen. J. Mater. Chem. A. 5, 7326 (2017).
14. B. V. Padlyak. Current Topics in Biophysics, 33 (suppl A), 163-170 (2010).
15. J. Even, L. Pedesseau, J-M Jancu, and C. Katan. J. Phys. Chem. Lett., 4, 2999−3005 (2013).
16. P. Xue, D. Pei, H. Zheng, W. Li, V. V. Afanas'ev, M. R. Baklanov, J-F de Marneffe c, Y-H Lin d, H-SumFung, C-chi Chend, Y Nishi, J. Leon Shohet. Thin Solid Films 616, 23–26 (2016).
17. F. Fungura, W. R. Lindemann, J. Shinar, and R. Shinar. Adv. Energy Mater., 7, 1601420-1601431 (2017).
18. S. Anderson., J. of Chem. Phys. 50, 2783 (1969).
19. Bogomolova, L.D., Zhachkin, V.A., Pavlushkina, T.K. Glass Ceram. Vol. 72, Nos. 3. (2015).

Downloaded from https://www.cambridge.org/core. IP address: 24.242.98.122, on 13 Feb 2018 at 03:49:54, subject to the Cambridge Core terms of use, available at https://www.cambridge.org/core/terms. https://doi.org/10.1557/adv.2018.171